Accepted Manuscript

Photoactivity improvement of TiO_2 electrodes by thin hole transport layers of reduced graphene oxide

Javier Hernández-Ferrer, Alejandro Ansón-Casaos, Sandra Víctor-Román, Olga Sanahuja-Parejo, M[a] Teresa Martínez, Belén Villacampa, Ana M. Benito, Wolfgang K. Maser

PII: S0013-4686(18)32792-0

DOI: https://doi.org/10.1016/j.electacta.2018.12.085

Reference: EA 33300

To appear in: *Electrochimica Acta*

Received Date: 26 October 2018

Revised Date: 12 December 2018

Accepted Date: 16 December 2018

Please cite this article as: J. Hernández-Ferrer, A. Ansón-Casaos, S. Víctor-Román, O. Sanahuja-Parejo, M.T. Martínez, Belé. Villacampa, A.M. Benito, W.K. Maser, Photoactivity improvement of TiO_2 electrodes by thin hole transport layers of reduced graphene oxide, *Electrochimica Acta* (2019), doi: https://doi.org/10.1016/j.electacta.2018.12.085.

This is a PDF file of an unedited manuscript that has been accepted for publication. As a service to our customers we are providing this early version of the manuscript. The manuscript will undergo copyediting, typesetting, and review of the resulting proof before it is published in its final form. Please note that during the production process errors may be discovered which could affect the content, and all legal disclaimers that apply to the journal pertain.

ACCEPTED MANUSCRIPT

Photoactivity improvement of TiO_2 electrodes by thin hole transport layers of reduced graphene oxide

Javier Hernández-Ferrer[a,*], Alejandro Ansón-Casaos[a], Sandra Víctor-Román[a], Olga Sanahuja-Parejo[a], Mª Teresa Martínez[a] , Belén Villacampa[b], Ana M. Benito[a], Wolfgang K. Maser[a]

[a]Instituto de Carboquímica ICB-CSIC, Miguel Luesma Castán 4, E-50018 Zaragoza, Spain

[b]Departamento de Física de La Materia Condensada, ICMA, Universidad de Zaragoza-CSIC, E-50009, Zaragoza, Spain

*Corresponding author: E-mail: jhernandez@icb.csic.es; Tel.: +34 976 733977

Abstract

Nanostructured TiO_2 and graphene-based materials constitute components of actual interest in devices related to solar energy conversion and storage. In this work, we show that a thin layer of electrochemically reduced graphene oxide (ECrGO), covering nanostructured TiO_2 photoelectrodes, can significantly improve the photoactivity. In order to understand the working principle, ECrGO/TiO_2 photoelectrodes with different ECrGO thicknesses were prepared and studied by a set of photoelectrochemical measurements. Methanol in alkaline conditions was employed as effective hole acceptor probe to elucidate the electronic phenomena in the electrode layers and interfaces. These studies underline the hole accepting properties of ECrGO and reveal the formation of a p-n junction at the interface between ECrGO and TiO_2. It is shown for

the first time that the resulting space charge region of about 10 nm defines the operational functionality of the ECrGO layer. Films thinner than the space charge region act as hole transport layer (HTL), which efficiently transfers holes to the liquid interface thus leading to enhanced photoactivity. Thicker films however act as hole blocking layer (HBL), resulting in a systematic decrease of the photoactivity. The finding of a thickness dependent threshold value for the operation of ECrGO as HTL and HBL is of general interest for the fabrication of optoelectronic devices with improved performance.

Keywords: titanium dioxide; reduced graphene oxide; photoelectrodes; hole-transport layer; photoelectrochemistry

1. Introduction

Photoelectrochemistry is a powerful tool to elucidate the performance and working mechanism of materials and interface components used in layered optoelectronic devices, such as thin film solar cells. The resulting data reveal critical information about electronic properties such as conduction and valence band limits, as well as trapping, distribution, separation, recombination and transport of charges [1, 2]. Using a simple electrochemical three-electrode configuration, photoelectrochemical measurements enable the elucidation of processes occurring at the working electrode, covering phenomena in bulk materials, across solid-solid interfaces for layered systems, as well as across the solid-liquid interface. Importantly, the acquired information provides valuable feedback for interface engineering towards optoelectronic device structures with improved performance.

Materials of great current interest for solar energy conversion and storage are metal oxides such as ZnO [3] or TiO_2 [2], as well as carbon nanomaterials (graphene-based materials and carbon nanotubes) [4]. Employed as photoelectrodes [5], electron transport layers (ETLs) [6] or hole transport layers (HTLs) [7], they constitute important components in optoelectronic devices. Especially TiO_2, graphene, and their hybrid materials are widely studied for this purpose [2, 8-12]. In dye-sensitized solar cells, TiO_2 is often used as the active layer, working as a photoanode [13, 14]. In the case of perovskite [15] and organic solar cells [6], TiO_2 can constitute ETL [16, 17], enabling the transfer of photogenerated electrons from the photoactive material to the conducting substrate. In new generation solar cells, reduced graphene oxide (rGO) layers can act as electron or hole acceptors [18, 19], protective layers [18], layers to improve the adhesion between polymeric and oxide layers [20, 21], and sensitizers absorbing light in the visible region [22-26]. However, systematic studies on thickness effects to elucidate the working principle of thin layers of reduced graphene oxide are yet missing.

This work investigates the photoelectrochemical properties of nanostructured TiO_2 films covered with electrochemically reduced graphene oxide (ECrGO) layers of different thicknesses. The films are used as photoelectrodes in a three-electrode electrochemical cell. Methanol in an alkaline solution is used as effective probe (effective hole acceptor enabling the direct methanol photo-oxidation process) for elucidating the electronic processes across the solid-liquid and solid-solid interfaces of the working electrode. Cyclic voltammetry under dark and illuminated conditions, time-dependent photocurrent and photovoltage measurements, as well as electrochemical impedance

spectroscopy clearly reveal that ECrGO layers act as acceptors of photo-induced holes from TiO_2 resulting in the formation of a p-n junction at the interface between ECrGO and TiO_2 comprising a space charge region of about 10 nm. For ECrGO layers up to 10 nm in thickness, this region extends into the solid-liquid interface, enhancing the photoelectroactivity of the electrode, thus acting as hole transport layer (HTL). Contrariwise, for thicker ECrGO layers photo-generated holes cannot reach anymore the solid-liquid interface and get blocked. Hence ECrGO layers with higher thicknesses act as hole blocking layer (HBL). These findings give us, for the first time, a benchmark for the use of ECrGO as either HTL or HBL in order to achieve optoelectronic structures with improved performance.

2. Experimental and methods

2.1. Materials and equipment

Commercial TiO_2 nanoparticles (Aeroxide P25, Evonik) were used in this work. Graphite flakes were purchased from Aldrich (ref. 332461). Reagent grade NaOH was bought from Sigma Aldrich. Ethanol and isopropanol (p.a. grade) were obtained from Panreac. Methanol (analytical reagent grade) was acquired from Fisher Scientific. Soda lime glass substrates, coated with fluorinated tin oxide (FTO, 70-100 Ω/sq, thickness of 80 nm, cut in 2.5x1 cm pieces) were shopped from Solems, Palaiseau, France. A graphite rod obtained from Cymit Quimica S.L., Barcelona, Spain, was used as the counter electrode. All the electrochemical measurements were performed in a three-electrode cell fitted with a quartz window, using an Autolab PGSTAT302N.

Illumination was carried out using a 150 W Xe arc lamp from LOT-Oriel (Germany), providing a measured light intensity of 300 $mW \cdot cm^{-2}$.

2.2 Electrode preparation

The electrode preparation process consists of 3 main stages: TiO_2 deposition, GO deposition, and GO electrochemical reduction (Figure S1, Supplementary data). First of all, FTO substrates were sonicated in isopropanol for 5 min. Blank TiO_2 films were prepared by spraying 1 mL of a TiO_2 suspension in absolute ethanol (2 mg/mL) onto approximately 1 cm^2 of the FTO substrate. Subsequently, the sample was thermally treated at 450ºC for two hours in N_2 atmosphere. The resulting TiO_2 films were 1.3-1.5 μm thick, as determined with a profilometer (Bruker DektakXT Stylus).

GO was synthesized from graphite flakes by a modified Hummers method including the following stages: i) overnight treatment in $NaNO_3/H_2SO_4/KMnO_4$ at 35ºC [27, 28], ii) cooling in 30% H_2O_2, iii) filtration, washing with diluted HCl and drying, and iv) resuspension in water at 0.5 $mg \cdot mL^{-1}$ and exfoliation in an ultrasounds bath for 2 h, final oxygen content, as measured by XPS, was 30.3 % w/w.

GO was deposited onto TiO_2 films employing an automatized spray coater (Nadetech ND-SP, Pamplona, Spain). Four GO/TiO_2 electrodes were spray-coated from 1, 2, 5 and 15 mL of the GO dispersion aliquots, resulting in GO films of 5, 10, 20, and 60 nm, respectively. The GO films were electrochemically reduced applying four potentiodynamic cycles between -0.040 and -1.440 V vs. Hg/HgO 0.1M KOH [12, 29, 30] (Figure S2, Supplementary data) affording the final ECrGO/TiO_2 electrodes studied in this work, with an oxygen content of 17.7 %, determined by XPS, in the case of 60

nm ECrGO/TiO_2 electrode. The electrodes are translucent and allow for measurements in transmittance mode.

C1s XPS spectra for the initial GO material and the final electrode are shown in figure S2.

2.3. Physicochemical characterization

Scanning electron microscopy (SEM) studies were carried out with a Hitachi S3400 N. Atomic force microscopy (AFM) measurements were performed with a Multimode SPM from Veeco Instruments (Santa Barbara, US) equipped with Nanoscope V controller and J-scanner. Images were acquired in tapping mode using antimonium (n)-doped Si tips RTESPA PART MPP-11120. Roughness analysis was carried out using the Nanoscope Analysis Version 1.5 software (Veeco Ins). Optical absorption spectroscopy in the near ultraviolet-visible (UV-Vis) range was performed in transmittance mode using a Shimazdu UV-2401 PC spectrometer. Data representation in form of Tauc-plots with exponent 0.5 for indirect allowed transitions was used to determine the optical absorption edges. Absorption edges were corrected using the background absorption from 1.4 to 1.9 eV as baseline in order to compensate for scattering effects [31]. XPS measurements were performed in a ESCAPlus spectrometer (OMICRON GmbH, Germany) using a Mg anode (1253.6 eV) operating at 225W (15mA, 15kV). Valence band edges were determined as crossing point of the linear baseline with the fitted linear line of the low energy linear part of the valence band.

2.4. Photoelectrochemical measurements

All the (photo)electrochemical measurements were performed using N_2-purged 0.1 M NaOH (pH=13) as the supporting electrolyte, to which 0.1 M methanol was added as hole acceptor, a Hg/HgO (0.1 M KOH) reference electrode and a graphite rod as the counter electrode. The scan rate was 20 $mV \cdot s^{-1}$ in all the cases. Two voltammetric cycles were performed, in order to achieve stationary conditions, and the second cycle is here presented. Photopotential was measured at zero current, according to $V_{ph} = E_{ph} - E_0$, where E_{ph} and E_0 are the open circuit potential (OCP) with and without the xenon lamp illumination respectively. In addition, the net photocurrent density j_{ph} is calculated from the voltammograms as the difference of the current density j between light and dark conditions at approximately -0.1 V vs. Hg/HgO, 0.1M KOH. Potentiostatic on-off chronoamperommetry was performed at 0.0 V (Hg/HgO, 0.1M KOH). Electrochemical impedance measurements were carried out from 10^5 to 10^{-2} Hz at the respective OCPs under the xenon lamp irradiation.

3. Results and discussion

3.1. Physical characterization

Aeroxide® P25 TiO_2 is a well-described standard material [32], while a complete characterization of GO and rGO materials can be found in our previous works [27, 28, 33-35]. Surface topography and optical absorption response, features of direct concern to the performance of the ECrGO/TiO_2 photoelectrodes, are detailed in the following. An AFM image of the blank TiO_2 electrode (Figure 1A) shows a quite uniform porous structure for TiO_2 films, with aggregates of about 300-400 nm uniformly distributed on the surface. The porous structure is essentially maintained for 5 nm and 10 nm

ECrGO/TiO_2 layers (Figure 1B), although the aggregates seem to be larger than in blank TiO_2 (about 600 nm) and the surface is less homogeneous. For 60 nm ECrGO/TiO_2, pore blocking due to the ECrGO layer thickness become evident (Figure 1C). The electrode surface is smoother than for blank TiO_2 and the spherical aggregates are not visible. In addition, AFM provides 3D quantitative information through the surface roughness parameters: S_a (average roughness evaluated over the complete 3D surface) and R_q (root mean square of height deviations taken from the mean image data plane (Table 1)). The S_a and R_q values are nearly identical for the blank TiO_2 and the 10 nm ECrGO/TiO_2 electrode, decreasing for electrodes with the thickest ECrGO layers. Finally the ECrGO layer becomes thick enough to block completely the porous structure of TiO_2. All the AFM observations were confirmed by scanning electron microscopy images (Figure S3, Supplementary data). AFM and SEM results suggest the TiO_2 surface is almost entirely covered by ECrGO, and thus, the solid/liquid interface will be mainly constituted between ECrGO and the electrolyte. These results are in agreement with SEM observations (Figure S3, Supplementary data).

The optical properties of the translucent ECrGO/TiO_2 photoelectrodes were analyzed by UV-Vis spectroscopy in transmittance mode (Figure S4, Supplementary data). A Tauc-plot representation of the acquired spectra is shown in Figure 2, The TiO_2 electrode reveals an absorption peak at 3.9 eV, and an absorption edge at 3.20 eV, (Figure 2) in agreement with the literature value for the indirect bandgap of TiO_2 [36]. In ECrGO/TiO_2 electrodes, both the absorption peak and the edge shift to lower energies with respect to the blank TiO_2 electrode. The lowest value of the absorption edge (2.70 eV) corresponds to the 5 nm ECrGO/TiO_2 electrode, and it subsequently increases with the thickness of the deposited ECrGO film (Table S1, Supplementary data).

While effects related to scattering from TiO_2 or the absorption from ECrGO are discarded as reasons for the observed shifts of the absorption edges, (see experimental details, as well as Supplementary data on Transmittance spectra, Figure S4), ECrGO layers most likely introduce a surface modification that strongly affects the electronic interactions between the ECrGO and TiO_2 interface. This may involve charge-transfer or/and space charge phenomena being responsible for the observed thickness dependent changes of the absorption levels of the nanostructured semiconducting electrodes [11, 23, 37, 38], as will be discussed in more detail in section 3.2.

On the other hand, valence band XPS spectra (Figure 3) show no change in the position and structure of TiO_2 valence band. These results indicate that the optical absorption properties (Figure 2), involve almost exclusively electronic levels close to the one of the conduction band of TiO_2.

3.2 Cyclic Voltammetry

3.2.1 Dark Voltammograms

An electrochemical study under dark conditions was performed for the description of the electrode interfaces in equilibrium state. In agreement with previous literature works [2], the dark voltammogram for the TiO_2 electrode in the supporting electrolyte exhibits an accumulation region at potentials lower than -1.1 V, a small feature due to electronic trap states at -0.7 V, and a depletion region at higher potentials (Figure 4). The ECrGO/TiO_2 electrodes show three significant changes compared to blank TiO_2:

- The accumulation region is shifted towards negative potentials (Figure 4B), reflecting an increase in the apparent energy of the conduction band edge, due to a negative charge accumulation in TiO_2. According to literature [39], this effect is assigned to an increase in the number of occupied Ti(III) states. Consequently, in ECrGO/TiO_2 electrodes, ECrGO would constitute a positively charged layer, thus, increasing the negative charge on TiO_2 surface [2, 11, 40]. The increase of their electron density through an effective charge transfer, thus shifts the measured conduction band edge towards more negative potentials[39, 40]. This charge separation between ECrGO and TiO_2, also predicted using ab-initio calculations [23, 41], constitutes the first evidence of the formation of a p-n junction between TiO_2 and ECrGO.

- A redox feature centered at -0.9 V increases with the rGO thickness until a nearly constant charge density (15, 20, 60 and 66 $\mu C \cdot cm^{-2}$ for the 5, 10, 20 and 60 nm ECrGO/TiO_2 electrodes, respectively; Figure S5A, Supplementary data). It can be assigned to electron trapping [42] at the interface between TiO_2 and ECrGO.

- An increase in the capacitive current takes place in the depletion region (E > -0.9 V), which is ascribed to an increase in the electrochemical capacitance due to the presence of ECrGO in contact with the electrolyte (Figure S5B, Supplementary data).

Next, changes taking place in the system upon the addition of methanol will be considered. Its value as effective probe for elucidating the electronic processes across

the solid-liquid and solid-solid interfaces will be discussed in the following sections. Figure 5A shows cyclic voltammetry measurements for the ECrGO/TiO_2 electrodes, before and after the addition of 0.1 M methanol. Blank TiO_2 experiences a negative shift in the accumulation region, demonstrating the adsorption of methanol and its role as electron donor to TiO_2. On the contrary, a large positive shift (140 mV) is observed for the 5 nm ECrGO/TiO_2 electrode, which is an indication of a strong interaction between methanol and ECrGO. Methanol is adsorbed as electron donor (or hole acceptor) on ECrGO [43], thus decreasing the quantity of positive charge in the layer, and consequently the electron transfer to the TiO_2 layer underneath, causing a displacement of the observed conduction band level towards positive potentials[40, 44]. The positive shift decreases for the 10 nm ECrGO/TiO_2 electrode (60 mV), and finally it almost disappears for the 20 nm ECrGO/TiO_2 electrode (10 mV), showing that, beyond a given film thickness, charge separation across the TiO_2/ECrGO interface is much less efficient.

The observed thickness effect is related to the spatial extension of the space charge built-up at the interface between the ECrGO and the TiO_2 layer. Its width can be estimated using equation (1), typically employed for p-n junctions [45]:

$$W_{sc} = \sqrt{\frac{2\phi\varepsilon}{eN_D}} \qquad (1)$$

where W_{sc} is the width of the space charge layer, ϕ is the potential drop across the interface between ECrGO and electrolyte (or TiO_2), e is the elementary charge and N_D is the carrier concentration. Typically, W_{sc} for graphite is 1 nm (three atomic layers) [45]. Taking then into account that the measured through-plane permittivity is 25 times

higher for rGO than for graphite [46], and N_D is typically 3-4 times higher for graphene than for rGO (10^{13} [47] vs. $3 \cdot 10^{12}$ [48]), one can roughly estimate the space charge layer thickness of ECrGO to be in the range from 8 to 10 nm. Although being a very rough first approximation, it reveals that for our thinnest ECrGO coatings, the, space charge layer thickness is larger than the ECrGO layer thickness itself. Consequently, the space charge width for ECrGO layers of 5 to 10 nm in thickness extends into the adjacent external interface layer (i.e. the adsorbed methanol) and thus favorably influences on the photoelectrochemical properties, as discussed in section 3.2.2. On the contrary, for ECrGO layers with thicknesses beyond 10 nm, the space charge width remains within the ECrGO layer, resulting in a decreased photoactivity.

Finally, Trap states at ~ 0.9 V shift in the presence of methanol, following a trend analogous to the conduction band edge.

A semi-quantitative calculation of the lowest energy level of the TiO_2 conduction band can be performed from the voltammetry measurements. The conduction band positions for the ECrGO/TiO_2 electrodes were calculated as the relative differences between linear regions in a plot of log(*C*) vs. *E*, where the capacitance per surface area is determined as $C=j \cdot (scan\ rate)^{-1}$ (Table S1, and Figures S5B and S6B, Supplementary data) [40]. In order to obtain an absolute value for the band edges, the position of blank TiO_2 in methanol was set to -1.40 V vs. Hg/HgO 0.1M KOH, according to a literature value [2]. In this way, a comparative graph for the conduction band edge is constructed for the ECrGO/TiO_2 electrodes in the presence of methanol (Figure 5B). The TiO_2 conduction band shifts to less negative potentials in the 5 nm ECrGO/TiO_2 electrode

compared to the TiO_2 electrode. However, as the thickness increases, the conduction band edge, systematically, goes again to more negative potentials, following a clear trend. This, once more, clearly underlines the importance of the thickness of the ECrGO layers for the overall electrochemical performance of the ECrGO/TiO_2 electrodes.

3.2.2. Photoelectrochemistry under illumination in the presence of methanol

Figure 6A shows cyclic voltammetry measurements in the presence of methanol. The steep increase in the current corresponds to methanol photo-oxidation. A half wave potential $E_{1/2}$ can be defined as the potential required for reaching a half of the maximum photocurrent density j_{ph}. The $E_{1/2}$ values are listed in Table 2, together with j_{ph}. The $E_{1/2}$ for 5 nm ECrGO/TiO_2, 10 nm ECrGO/TiO_2 and 20 nm ECrGO/TiO_2 are lower than for the bare TiO_2 electrode. An increase in the j_{ph} of 14% and 9% is obtained for the 5 and 10 nm ECrGO/TiO_2 electrodes respectively. When ECrGO layers become thicker, j_{ph} starts to decrease with film thickness, and it is almost completely blocked in the 60 nm ECrGO electrode. Only in thin ECrGO/TiO_2 electrodes, photogenerated holes are efficiently transferred from TiO_2 to the valence band of ECrGO layer, in agreement with its behavior as hole acceptor observed in section 3.2.1. Methanol in solution is able to capture photo-holes, providing an electron to ECrGO, and improving j_{ph} and $E_{1/2}$ compared to TiO_2. When performing potentiostatic on-off photocurrent measurements at 0.0 V (Figure 6B), it can be observed that the photocurrent is rather stable with time. However, the stability gets further improved due to the presence of the ECrGO layers, in agreement with observations for GO and rGO in solar energy systems [6, 18]. Photocurrent decreases from $j_{(t=15s)}$= 136 $\mu A \cdot cm^{-2}$ to $j_{(t=290s)}$= 129 $\mu A \cdot cm^{-2}$ (5.1 %) in the case of TiO_2, and from $j_{(t=15s)}$= 151 $\mu A \cdot cm^{-2}$ to $j_{(t=290s)}$= 149 $\mu A \cdot cm^{-2}$ (1.3%) in the

case of 5 nm ECrGO/TiO_2 electrode, remaining essentially constant for 10 nm ECrGO/TiO_2 electrode. At t=290 s, the increase in photocurrent, with respect to the TiO_2 electrode, is 16% for 5 nm ECrGO/TiO_2 and 11% for 10 nm ECrGO/TiO_2.

The increase in halfwave potential and photocurrent implies improved charge separation and, once more, suggests the formation of a p-n junction, as also described in the literature for similar TiO_2/rGO systems [22, 49]. In these systems, photoelectrons remain in TiO_2, while photoholes move to rGO (ECrGO in our case). As rGO is in contact with the solution, the holes are more likely to be transferred to the molecules of the liquid phase. The formation of a p-n junction has been observed to provide a significant decrease in the onset potential for water photooxidation, not only for rGO films, but also with inorganic semiconductor layered systems, such as CoO_x/TiO_2 [50, 51], TiO_2/hematite [52, 53] and WO_3/FeOOH [54] electrodes.

In agreement with previous reports, the photocurrent for methanol oxidation is higher than for water oxidation [55]. Actually, although the halfwave potential is more negative, the water oxidation photocurrent in ECrGO/TiO_2 electrodes decreases compared to blank TiO_2, indicating that water molecules do not efficiently react with photogenerated holes, most probably due to the hydrophobic nature of graphene basal plane [56] (Figure S7 and Table S2, Supplementary data). Therefore, when ECrGO forms part of the electrode-solution interface, the interaction between water and ECrGO active sites is not efficient to favor charge transport towards the liquid phase. On the contrary, when methanol is present in the solution, strong interactions with the electrode surface are achieved [56-58] and an improvement in both the halfwave potential and the photocurrent is obtained.

As can be seen from these results key issues for achieving improved photoactivity in layered ECrGO/TiO_2 photoelectrodes refer to: (a) the formation of favorable solid-liquid interface interactions (provided by methanol acting as hole acceptor), (b) the establishment of a p-n junction at the solid-solid interface between the hole-accepting ECrGO and the TiO_2 layers, and a corresponding space charge region which extends into the adjacent solid-liquid interface and thus enables effective hole transport to the neighboring hole-accepting (methanol) layer. This is ensured whenever ECrGO thickness < W_{sc} thickness. This threshold criterion is responsible for the observed thickness effects.

3.3 Photopotential measurements

Open circuit potential (OCP) in the dark provides an estimation of the Fermi level energy of the electrode and, in the absence of any reversible redox couple, it is determined kinetically by all the processes occurring at the electrode [2]. For ECrGO/TiO_2 electrodes in 0.1 M NaOH + 0.1 M methanol, the OCP in the dark is higher than for TiO_2, indicating that the combined effects of methanol and ECrGO layers decrease the electron energy in the system.

Figure 7 shows the evolution of OCP during 3 min. The electrodes are exposed to xenon lamp irradiation for 50 s, and then the lamp is switched off. The photopotential is defined as the difference between OCPs under illumination and initial in the dark ($V_{ph}=E_{ph}-E_0$), and it is directly related to the quantity of photogenerated electron-hole pairs. The value of E_{ph} for a photoanode is associated to the excess of electrons in the

conduction band, while holes are transferred to the solution, and it is only limited by the energy level of the conduction band [2]. The measured E_{ph} and V_{ph} values are listed in Table 2. For the 5 nm ECrGO/TiO_2 electrode, E_{ph} is 5% less negative and V_{ph} is 44% higher with respect to blank TiO_2. Therefore, a higher quantity of electron-hole pairs is separated. For 10 and 20 nm ECrGO/TiO_2 electrodes, V_{ph} and E_{ph} are also higher (in absolute values) than the respective values for TiO_2. Moreover, the 20 nm ECrGO/TiO_2 electrode shows the highest V_{ph}. However, it needs the longest time to reach a stationary E_{ph} value, i.e. the processes that govern photoactivity are slow, and thus a decrease in the j_{ph} is observed. For 60 nm ECrGO/TiO_2, the processes are so slow that no stationary photopotential is reached in the time range. These results further underline that ECrGO layers act as hole acceptors from TiO_2 and thus efficiently contribute to improved charge separation. For thin films holes can be transferred to the subsequent hole acceptor molecule (i.e. methanol) leading to enhanced photoactivity. In this situation ECrGO assumes the function of a hole transport layer (HTL). For thick films holes get blocked in the ECrGO layer, and photoactivity decreases with film thickness. Under this circumstance, ECrGO plays the role of a hole-blocking layer (HBL). The overall mechanism is summarized in Scheme 1.

3.4 Electrochemical Impedance Spectroscopy

Potentiostatic impedance spectra in 0.1 M NaOH + 0.1 M methanol were performed at the respective OCPs under illumination for the 5 nm, 10 nm and 20 nm ECrGO/TiO_2 electrodes, as well as for the bare TiO_2 electrode (Figure 8), and fitted to the equivalent circuit shown in Figure S7, commonly used for the description of the behavior of semiconductor electrodes [59]. The impedance spectra for TiO_2 and ECrGO/TiO_2 are

qualitatively similar, and fit to the same equivalent circuit. This suggests that the electrode/solution interface is only constituted by one single component, whereby essentially only ECrGO is in contact with the solution, in agreement with SEM and AFM results. Areas of non-covered TiO_2 eventually may be in direct contact with the solution, but their influence is estimated to be negligible. The modulus Bode plot is shown in Figure 8A and the phase Bode plot is in Figure 8B. At intermediate frequencies around 10^2 Hz, a small feature appears in all the samples, which can be tentatively ascribed to the FTO exposed to the electrode (charge transfer resistance R1, in parallel with capacitance Q1, of FTO exposed zones[60]). At low frequencies, the phase Bode plot for the TiO_2 electrode shows a peak centered at 0.08 Hz, which describes the intrinsic behavior of the film (charge-transfer resistance R2 in parallel with the chemical capacitance of the film Q2, see Figure S8, Supplementary Data, and [1, 60]). The peak shifts for the ECrGO/TiO_2 films, indicating changes in the total capacitance of the film (Table S3, Supplementary data). Impedance modulus for 5 nm and 10 nm ECrGO/TiO_2 is higher than impedance modulus for TiO_2 at frequencies higher than 0.1 Hz. On the contrary, at lower frequencies, impedances for 5 nm ECrGO ($1.2\cdot10^4\,\Omega$) and 10 nm ECrGO/TiO_2 ($4.6\cdot10^3\,\Omega$) electrodes are significantly lower than for TiO_2 ($2.6\cdot10^4\,\Omega$). The decrease in the impedance modulus is associated with low phase angles, thus indicating that charge transfer at the electrode is much faster for TiO_2 electrodes covered with thin ECrGO layers, in agreement with the findings described above. For rGO layers as thick as 20 nm, the positive effect is lost. The 10 nm ECrGO/TiO_2 electrode presents the best charge transfer properties (the lowest impedance) among the studied materials. The low value of OCP under illumination (E_{ph}) (Section 3.3) plays a key role and leads to a clear improvement in the TiO_2 behavior as the photoanode of photocatalytic and photovoltaic systems.

4. Conclusions

Photoelectrochemical measurements in the presence of methanol show that a thin ECrGO covering layer significantly improves the photopotential (up to 270 mV), halfwave potential (up to 120 mV) and photocurrent (up to ca. 16%) of nanostructured TiO_2 electrodes. These results reveal that the mechanism behind this process is based on (a) the formation of a favorable solid-liquid interface. This is ensured by the use of methanol as well adsorbing hole acceptor; (b) the establishment of a p-n junction at the solid-solid interface between the hole-accepting ECrGO coating layer and the TiO_2 layer underneath. Here the width of the built-up space charge region of about 10 nm defines a clear threshold criterion for the operational functionality of the ECrGO coating layer and the photoactivity of the overall ECrGO/TiO_2 photoelectrode. For ECrGO layers with thicknesses smaller than the width of the space charge region, the space charge region extends into the solid-liquid interface. This favors hole-transport to hole accepting methanol resulting in enhanced photoactivity of the photoelectrode. In this scenario ECrGO acts as hole transport layer (HTL) When the thickness of the ECrGO coating layer exceeds the width of the space charge region holes get blocked in the ECrGO layer leading to a decreased photoactivity. Here ECrGO acts as hole blocking layer (HBL). These findings for the first time establish a general criterion for the use of (electrochemically) reduced graphene oxide as either HTL or HBL as component in layered optoelectronic device structures thus being of general relevance for the fabrication of devices with improved performance.

Acknowledgements

The authors thank Prof. M.T. Martínez for AFM measurements and the Analysis Service of the Instituto de Carboquímica (ICB-CSIC) for XPS measurements. This work has received funding from the Spanish MINEICO (project grant ENE 2016-79282-C5-1-R), Gobierno de Aragón *(Grupo Reconocido* DGA T03_17R), and associated EU Regional Development Funds. S.V. acknowledges Spanish MINEICO for her PhD grant (BES2014-068727 and associated EU Social Funds).

References

[1] F. Fabregat-Santiago, I. Mora-Seró, G. Garcia-Belmonte, J. Bisquert, Cyclic voltammetry studies of nanoporous semiconductors. Capacitive and reactive properties of nanocrystalline TiO_2 electrodes in aqueous electrolyte, J. Phys. Chem. B, 107 (2003) 758-768.

[2] T. Berger, D. Monllor-Satoca, M. Jankulovska, T. Lana-Villarreal, R. Gómez, The electrochemistry of nanostructured titanium dioxide electrodes, ChemPhysChem, 13 (2012) 2824-2875.

[3] S. Shet, Zinc Oxide (ZnO) Nanostructures for Photoelectrochemical Water Splitting Application, ECS Transactions, 33 (2011) 15-25.

[4] D. Chen, H. Zhang, Y. Liu, J. Li, Graphene and its derivatives for the development of solar cells, photoelectrochemical, and photocatalytic applications, Energ. Environ. Sci., 6 (2013) 1362-1387.

[5] R. Memming, Semiconductor Electrochemistry, 2nd Edition, WILEY‐VCH Verlag GmbH2015.

[6] A. Morais, J.P.C. Alves, F.A.S. Lima, M. Lira-Cantu, A.F. Nogueira, Enhanced photovoltaic performance of inverted hybrid bulk-heterojunction solar cells using TiO_2/reduced graphene oxide films as electron transport layers, J. Photon. Energy, 5 (2015).

[7] X. Huang, H. Yu, Z. Wu, Y. Li, Improving the performance of polymer solar cells by efficient optimizing the hole transport layer-graphene oxide, J. Solid State Electrochem., 22 (2018) 317-329.

[8] J. Chen, F. Qiu, W. Xu, S. Cao, H. Zhu, Recent progress in enhancing photocatalytic efficiency of TiO_2-based materials, Appl. Catal. A-Gen., 495 (2015) 131-140.

[9] R. Leary, A. Westwood, Carbonaceous nanomaterials for the enhancement of TiO_2 photocatalysis, Carbon, 49 (2011) 741-772.

[10] Y. Bai, I. Mora-Seró, F. De Angelis, J. Bisquert, P. Wang, Titanium Dioxide Nanomaterials for Photovoltaic Applications, Chem. Rev., 114 (2014) 10095-10130.

[11] J. Schneider, M. Matsuoka, M. Takeuchi, J. Zhang, Y. Horiuchi, M. Anpo, D.W. Bahnemann, Understanding TiO_2 Photocatalysis: Mechanisms and Materials, Chem. Rev., 114 (2014) 9919-9986.

[12] T. Kuila, A.K. Mishra, P. Khanra, N.H. Kim, J.H. Lee, Recent advances in the efficient reduction of graphene oxide and its application as energy storage electrode materials, Nanoscale, 5 (2013) 52-71.

[13] X. Xu, D. Huang, K. Cao, M. Wang, S.M. Zakeeruddin, M. Grätzel, Electrochemically Reduced Graphene Oxide Multilayer Films as Efficient Counter Electrode for Dye-Sensitized Solar Cells, Sci. Rep., 3 (2013) 1489.

[14] M. Grätzel, Dye-sensitized solar cells, J. Photoch. Photobio. C, 4 (2003) 145-153.

[15] J. Carrillo, A. Guerrero, S. Rahimnejad, O. Almora, I. Zarazua, E. Mas-Marza, J. Bisquert, G. Garcia-Belmonte, Ionic Reactivity at Contacts and Aging of

Methylammonium Lead Triiodide Perovskite Solar Cells, Adv. Energy Mater., 6 (2016).

[16] S. Lattante, Electron and Hole Transport Layers: Their Use in Inverted Bulk Heterojunction Polymer Solar Cells, Electronics, 3 (2014) 132.

[17] R. Peng, F. Yang, X. Ouyang, Y. Liu, Y.-S. Kim, Z. Ge, Enhanced photovoltaic performance of inverted polymer solar cells by tuning the structures of titanium dioxide, Thin Solid Films, 545 (2013) 424-428.

[18] E. Singh, H.S. Nalwa, Stability of graphene-based heterojunction solar cells, RSC Adv., 5 (2015) 73575-73600.

[19] E. Singh, H.S. Nalwa, Graphene-Based Bulk-Heterojunction Solar Cells: A Review, J. Nanosci. and Nanotechno., 15 (2015) 6237-6278.

[20] T. Xu, Q. Qiao, Conjugated polymer-inorganic semiconductor hybrid solar cells, Energ. Environ. Sci., 4 (2011) 2700-2720.

[21] K. Shankar, G.K. Mor, H.E. Prakasam, O.K. Varghese, C.A. Grimes, Self-Assembled Hybrid Polymer−TiO_2 Nanotube Array Heterojunction Solar Cells, Langmuir, 23 (2007) 12445-12449.

[22] X. Zhang, Z. Chen, The enhanced photoactivity of hydrogenated TiO_2@reduced graphene oxide with p-n junctions, RSC Adv., 5 (2015) 26328-26334.

[23] A. Du, Y.H. Ng, N.J. Bell, Z. Zhu, R. Amal, S.C. Smith, Hybrid graphene/titania nanocomposite: Interface charge transfer, hole doping, and sensitization for visible light response, J. Phys. Chem. Lett., 2 (2011) 894-899.

[24] R. Kumar, R.K. Singh, P. Kumar Dubey, D.P. Singh, R.M. Yadav, R.S. Tiwari, Hydrothermal synthesis of a uniformly dispersed hybrid graphene-TiO_2 nanostructure for optical and enhanced electrochemical applications, RSC Adv., 5 (2015) 7112-7120.

[25] Y. Zhu, Y. Wang, W. Yao, R. Zong, Y. Zhu, New insights into the relationship between photocatalytic activity and TiO_2-GR composites, RSC Adv., 5 (2015) 29201-29208.

[26] A. Razzaq, C.A. Grimes, S.I. In, Facile fabrication of a noble metal-free photocatalyst: TiO_2 nanotube arrays covered with reduced graphene oxide, Carbon, 98 (2016) 537-544.

[27] C. Vallés, J. David Núñez, A.M. Benito, W.K. Maser, Flexible conductive graphene paper obtained by direct and gentle annealing of graphene oxide paper, Carbon, 50 (2012) 835-844.

[28] J.D. Nunez, A.M. Benito, S. Rouziere, P. Launois, R. Arenal, P.M. Ajayan, W.K. Maser, Graphene oxide-carbon nanotube hybrid assemblies: cooperatively strengthened OH···O=C hydrogen bonds and the removal of chemisorbed water, Chem. Sci., 8 (2017) 4987-4995.

[29] H.-L. Guo, X.-F. Wang, Q.-Y. Qian, F.-B. Wang, X.-H. Xia, A Green Approach to the Synthesis of Graphene Nanosheets, ACS Nano, 3 (2009) 2653-2659.

[30] Y. Shao, J. Wang, M. Engelhard, C. Wang, Y. Lin, Facile and controllable electrochemical reduction of graphene oxide and its applications, J. Mater. Chem., 20 (2010) 743-748.

[31] Z. Chen, T.F. Jaramillo, T.G. Deutsch, A. Kleiman-Shwarsctein, A.J. Forman, N. Gaillard, R. Garland, K. Takanabe, C. Heske, M. Sunkara, E.W. McFarland, K. Domen, E.L. Miller, J.A. Turner, H.N. Dinh, Accelerating materials development for photoelectrochemical hydrogen production: Standards for methods, definitions, and reporting protocols, J. Mater. Res., 25 (2011) 3-16.

[32] B. Ohtani, O.O. Prieto-Mahaney, D. Li, R. Abe, What is Degussa (Evonik) P25? Crystalline composition analysis, reconstruction from isolated pure particles and photocatalytic activity test, J. Photoch. Photobio. A, 216 (2010) 179-182.

[33] A. Tararan, A. Zobelli, A.M. Benito, W.K. Maser, O. Stéphan, Revisiting Graphene Oxide Chemistry via Spatially-Resolved Electron Energy Loss Spectroscopy, Chem. Mater., 28 (2016) 3741-3748.

[34] A. Ansón-Casaos, J.A. Puértolas, F.J. Pascual, J. Hernández-Ferrer, P. Castell, A.M. Benito, W.K. Maser, M.T. Martínez, The effect of gamma-irradiation on few-layered graphene materials, App. Surf. Sci., 301 (2014) 264-272.

[35] A.V. Dolbin, M.V. Khlistyuck, V.B. Esel'son, V.G. Gavrilko, N.A. Vinnikov, R.M. Basnukaeva, I. Maluenda, W.K. Maser, A.M. Benito, The effect of the thermal reduction temperature on the structure and sorption capacity of reduced graphene oxide materials, App. Surf. Sci., 361 (2016) 213-220.

[36] I.S. Grover, S. Singh, B. Pal, Stable anatase TiO_2 formed by calcination of rice-like titania nanorod at 800 ºC exhibits high photocatalytic activity, RSC Adv., 4 (2014) 24704-24709.

[37] H.I. Kim, G.H. Moon, D. Monllor-Satoca, Y. Park, W. Choi, Solar photoconversion using graphene/TiO_2 composites: Nanographene shell on TiO 2 core versus TiO_2 nanoparticles on graphene sheet, J. Phys. Chem. C, 116 (2012) 1535-1543.

[38] C. Zhai, M. Zhu, F. Ren, Z. Yao, Y. Du, P. Yang, Enhanced photoelectrocatalytic performance of titanium dioxide/carbon cloth based photoelectrodes by graphene modification under visible-light irradiation, J. Hazard. Mater., 263 (2013) 291-298.

[39] L.A. Lyon, J.T. Hupp, Energetics of the Nanocrystalline Titanium Dioxide/Aqueous Solution Interface: Approximate Conduction Band Edge Variations between $H_0 = -10$ and $H_- = +26$, J. Phys. Chem. B, 103 (1999) 4623-4628.

[40] J. Bisquert, F. Fabregat-Santiago, I. Mora-Seró, G. Garcia-Belmonte, E.M. Barea, E. Palomares, A review of recent results on electrochemical determination of the density of electronic states of nanostructured metal-oxide semiconductors and organic hole conductors, Inorg. Chim. Acta, 361 (2008) 684-698.

[41] L. Ferrighi, G. Fazio, C.D. Valentin, Charge Carriers Separation at the Graphene/(101) Anatase TiO_2 Interface, Adv. Mater. Interfaces, 3 (2016).

[42] L. Bertoluzzi, L. Badia-Bou, F. Fabregat-Santiago, S. Gimenez, J. Bisquert, Interpretation of Cyclic Voltammetry Measurements of Thin Semiconductor Films for Solar Fuel Applications, J. Phys. Chem. Lett., 4 (2013) 1334-1339.

[43] X.W. Zhao, Y.L. Tian, W.W. Yue, M.N. Chen, G.C. Hu, J.F. Ren, X.B. Yuan, Adsorption of methanol molecule on graphene: Experimental results and first-principles calculations, Int. J. Mod. Phys. B, 32 (2018) 1850102.

[44] F. Fabregat-Santiago, J. Bisquert, G. Garcia-Belmonte, G. Boschloo, A. Hagfeldt, Influence of electrolyte in transport and recombination in dye-sensitized solar cells studied by impedance spectroscopy, Sol. Energ. Mater. Sol. C., 87 (2005) 117-131.

[45] H. Gerischer, An interpretation of the double layer capacity of graphite electrodes in relation to the density of states at the Fermi level, J. Phys. Chem., 89 (1985) 4249-4251.

[46] X. Hong, W. Yu, D.D.L. Chung, Electric permittivity of reduced graphite oxide, Carbon, 111 (2017) 182-190.

[47] J. Ye, M.F. Craciun, M. Koshino, S. Russo, S. Inoue, H. Yuan, H. Shimotani, A.F. Morpurgo, Y. Iwasa, Accessing the transport properties of graphene and its multilayers at high carrier density, P. Natl. Acad. Sci. USA, 108 (2011) 13002-13006.

[48] G. Eda, C. Mattevi, H. Yamaguchi, H. Kim, M. Chhowalla, Insulator to Semimetal Transition in Graphene Oxide, J. Phys. Chem. C, 113 (2009) 15768-15771.

[49] J. Xu, J. Tian, Y. Zhang, A. Riaz, Y. Liu, M. Zhi, Z. Hong, C. Zhou, Carbonaceous layer interfaced TiO_2/RGO hybrids with enhanced visible-light photocatalytic performance, RSC Adv., 6 (2016) 40304-40311.

[50] F. Lin, B.F. Bachman, S.W. Boettcher, Impact of Electrocatalyst Activity and Ion Permeability on Water-Splitting Photoanodes, J. Phys. Chem. Lett., 6 (2015) 2427-2433.

[51] M.R. Nellist, F.A.L. Laskowski, F. Lin, T.J. Mills, S.W. Boettcher, Semiconductor–Electrocatalyst Interfaces: Theory, Experiment, and Applications in Photoelectrochemical Water Splitting, Accounts Chem. Res., 49 (2016) 733-740.

[52] H. Dotan, K. Sivula, M. Grätzel, A. Rothschild, S.C. Warren, Probing the photoelectrochemical properties of hematite (α -Fe_2O_3) electrodes using hydrogen peroxide as a hole scavenger, Energ. Environ. Sci., 4 (2011) 958-964.

[53] T. Hisatomi, H. Dotan, M. Stefik, K. Sivula, A. Rothschild, M. Grätzel, N. Mathews, Enhancement in the Performance of Ultrathin Hematite Photoanode for Water Splitting by an Oxide Underlayer, Adv. Mater., 24 (2012) 2699-2702.

[54] J. Huang, Y. Ding, X. Luo, Y. Feng, Solvation effect promoted formation of p–n junction between WO_3 and FeOOH: A high performance photoanode for water oxidation, J. Catal., 333 (2016) 200-206.

[55] D. Jiang, H. Zhao, Z. Jia, J. Cao, R. John, Photoelectrochemical behaviour of methanol oxidation at nanoporous TiO_2 film electrodes, J. Photoch. Photobio. A, 144 (2001) 197-204.

[56] O. Leenaerts, B. Partoens, F.M. Peeters, Water on graphene: Hydrophobicity and dipole moment using density functional theory, Phys. Rev. B, 79 (2009) 235440.

[57] E. Schröder, Methanol Adsorption on Graphene, J. Nanomater., 2013 (2013) 6.

[58] S. You, J. Yu, B. Sundqvist, L.A. Belyaeva, N.V. Avramenko, M.V. Korobov, A.V. Talyzin, Selective Intercalation of Graphite Oxide by Methanol in Water/Methanol Mixtures, J. Phys. Chem. C, 117 (2013) 1963-1968.

[59] T. Lopes, L. Andrade, F. Le Formal, M. Gratzel, K. Sivula, A. Mendes, Hematite photoelectrodes for water splitting: evaluation of the role of film thickness by impedance spectroscopy, Phys. Chem. Chem. Phys., 16 (2014) 16515-16523.

[60] F. Fabregat-Santiago, G. Garcia-Belmonte, I. Mora-Sero, J. Bisquert, Characterization of nanostructured hybrid and organic solar cells by impedance spectroscopy, Phys. Chem. Chem. Phys., 13 (2011) 9083-9118.

ACCEPTED MANUSCRIPT

Table 1. Roughness parameters calculated from AFM data.

Electrode	S_q/nm	S_a/nm
TiO_2	240	177
10 nm ECrGO/TiO_2	257	180
60 nm ECrGO/TiO_2	185	145

Table 2. Photoactivity parameters in 0.1 M NaOH + 0.1 M methanol.

Electrode	$E_{1/2}$/V	j_{ph}/μA·cm^{-2}	E_{ph}/V	V_{ph}/V
TiO_2	-0.97	136	-1.21	-0.61
5 nm ECrGO/TiO_2	-1.04	154	-1.15	-0.88
10 nm ECrGO/TiO_2	-1.09	148	-1.25	-0.85
20 nm ECrGO/TiO_2	-1.06	86	-1.25	-0.92
60 nm ECrGO/TiO_2	-0.99	3	-	-

ACCEPTED MANUSCRIPT

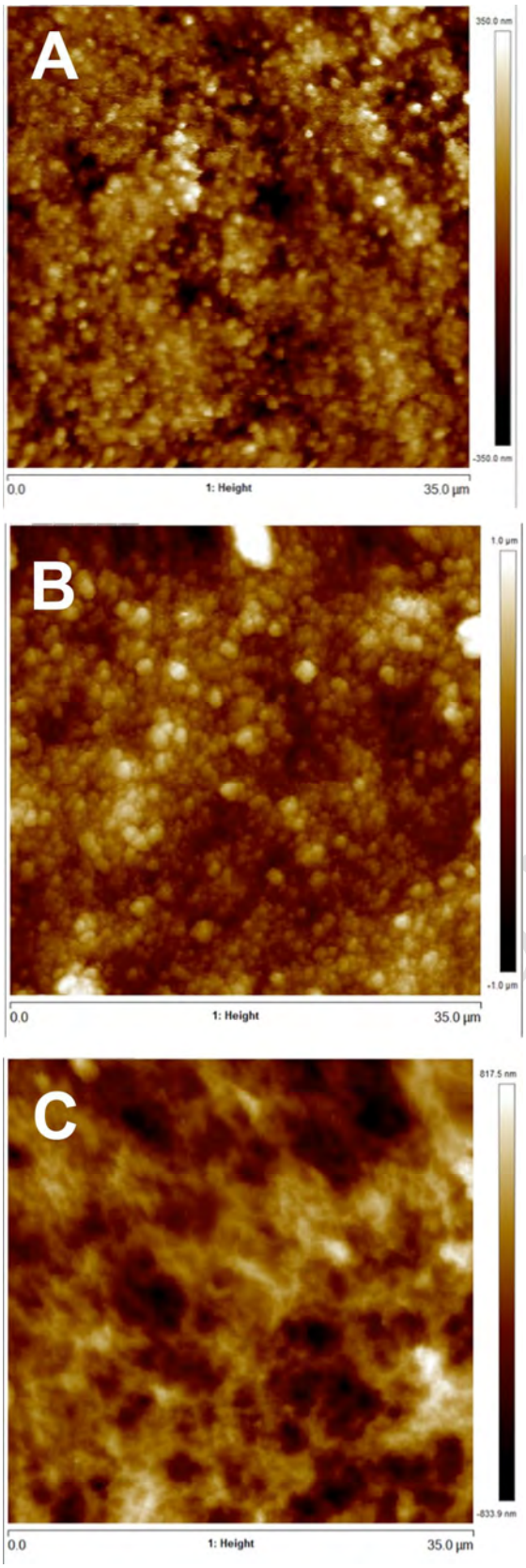

Figure 1. 35x35 µm AFM images of different electrodes: A) TiO_2, B) 10 nm ECrGO/TiO_2, and C) 60 nm ECrGO/TiO_2.

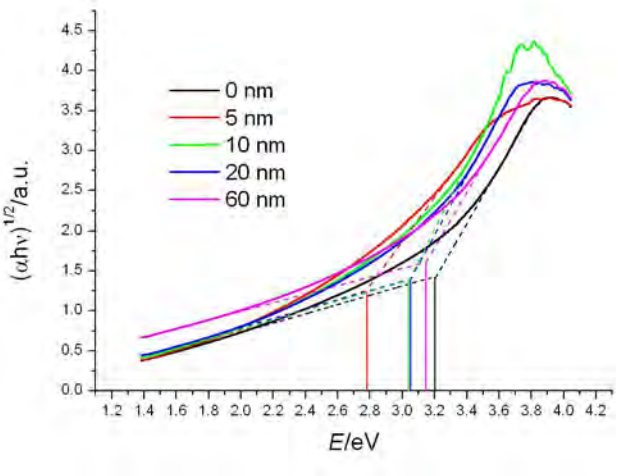

Figure 2. Tauc plot for the TiO_2 and ECrGO/TiO_2 electrodes.

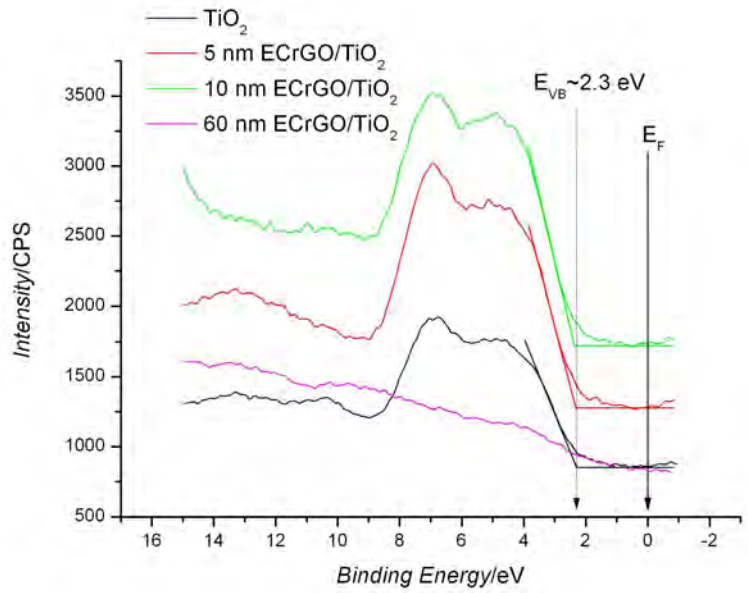

Figure 3. Valence band XPS spectra for the TiO_2 and ECrGO/TiO_2 electrodes.

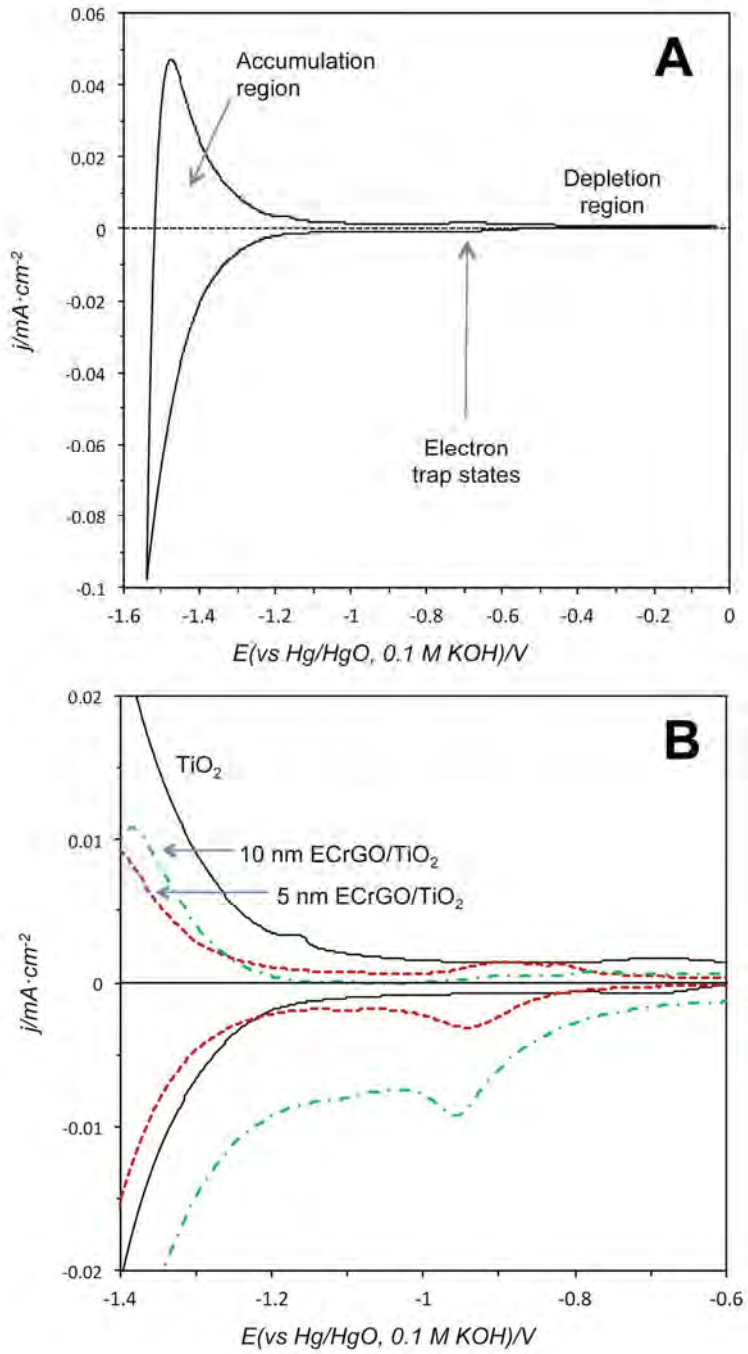

Figure 4. Cyclic voltammetry in dark conditions (0.1 M NaOH, v=20 $mV \cdot s^{-1}$): A) Blank TiO_2 indicating the voltammogram main regions; and B) TiO_2 compared to the ECrGO/TiO_2 electrodes with the thinnest ECrGO films.

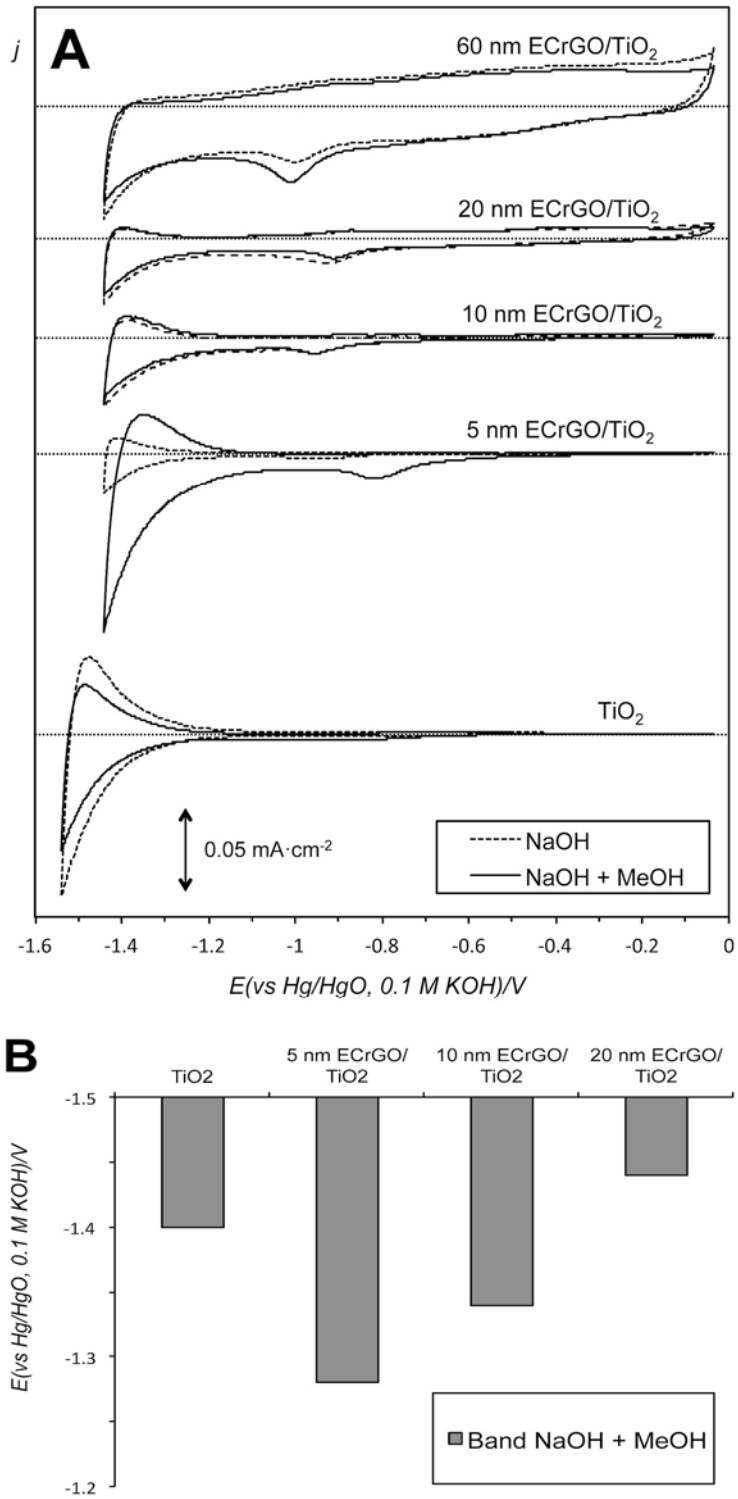

Figure 5. Electrochemical characterization in dark conditions for the TiO_2 and ECrGO/TiO_2 electrodes: A) Cyclic voltammetry in 0.1 M NaOH and 0.1 M NaOH + 0.1 M methanol (v=20 $mV \cdot s^{-1}$); and B) approximate position of the TiO_2 conduction band.

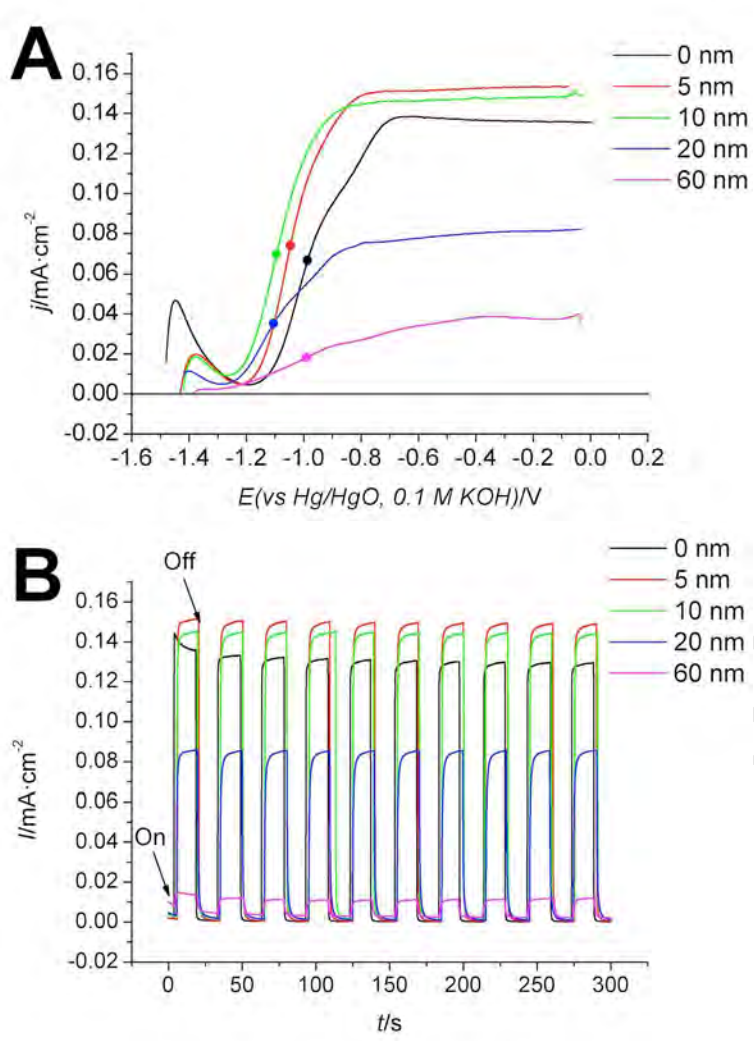

Figure 6. (A) Cyclic voltammograms (anodic sweep) at 20 $mV \cdot s^{-1}$ under illumination and (B) chronoamperograms at 0.4 V for the TiO_2 and ECrGO/TiO_2 electrodes in 0.1 M NaOH + 0.1 M MeOH.

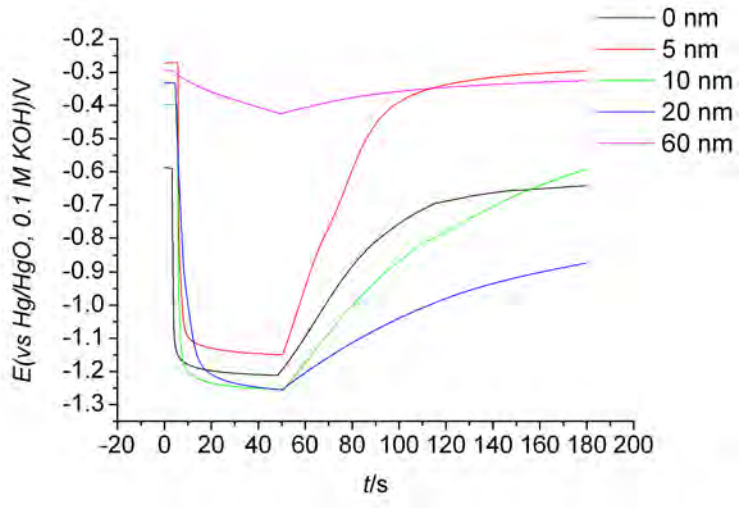

Figure 7. Photopotential measurements for the TiO_2 and ECrGO/TiO_2 electrodes in 0.1 M NaOH + 0.1 M methanol.

ACCEPTED MANUSCRIPT

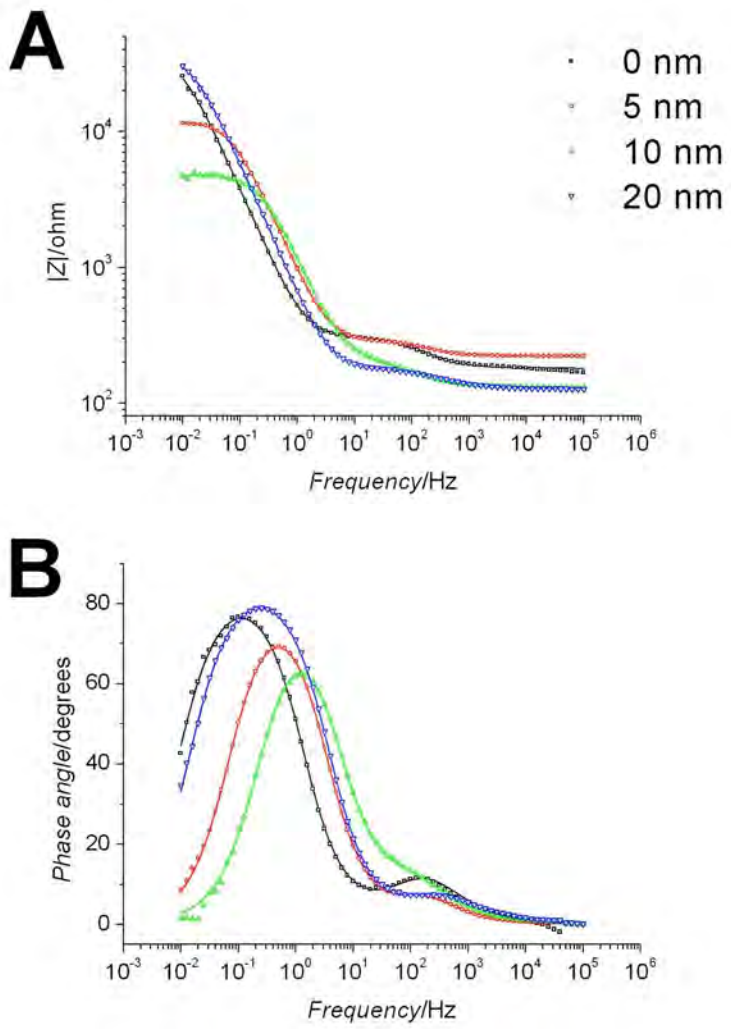

Figure 8. Electrochemical impedance spectroscopy for the TiO_2 and ECrGO/TiO_2 electrodes under illumination in 0.1 M NaOH + 0.1 M methanol: A) impedance modulus Bode plot, and B) phase Bode plot. Measurements were performed at the respective OCP: -1.31 V for TiO_2, -1.06 V for 5 nm ECrGO/TiO_2, -1.13 V for 10 nm ECrGO/TiO_2, and -1.22 V for 20 nm ECrGO/TiO_2.

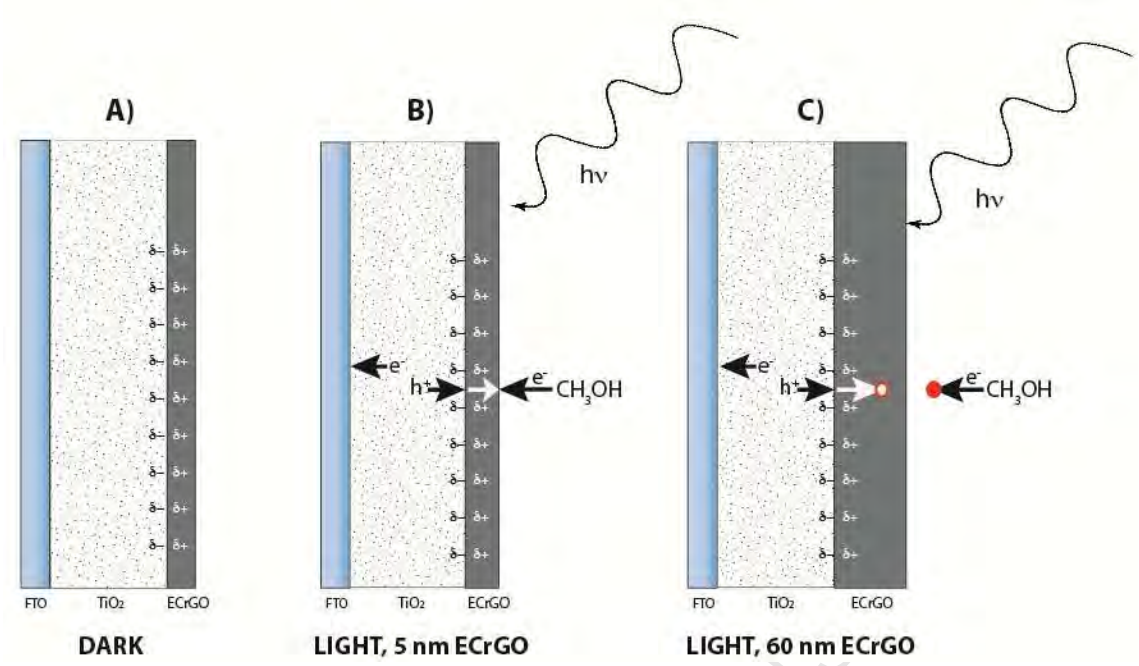

Scheme 1. Interpretation of the photocatalytic mechanism of methanol oxidation on ECrGO/TiO_2 electrodes: A) in the dark, partial negative charges (δ-) accumulate on TiO_2, and partial positive charges (δ+) accumulate on ECrGO. Under illumination, electrons and holes are generated at TiO_2, and photo-holes are transferred to ECrGO: B) if the ECrGO layer is thinner than the space charge layer, the hole is able to react with methanol and the ECrGO layer acts as a hole-transport layer; C) if the ECrGO layer is thicker than the space charge layer, the hole cannot reach the solution and ECrGO acts as a blocking layer.

ACCEPTED MANUSCRIPT